Electronic Supplementary Material (ESI) for Inorganic Chemistry Frontiers.

Electronic Supporting Information

Organic–Inorganic hybrid phosphite-participating *S*-shaped penta-Ce^{III} incorporated tellurotungstate as electrochemical enzymatic hydrogen peroxide for β-D-Glucose detection

Nizi Song, Yanzhou Li,* Yanying Wang, Menglu Wang, Mengling Liu, Lijuan Chen,* Junwei Zhao*

Henan Key Laboratory of Polyoxometalate Chemistry, College of Chemistry and Chemical Engineering, Henan University, Kaifeng 475004, China

Fig. S1. Illustration of some typical HNLITTs. (a) $[\{(TeO_3)W_{10}O_{34}\}_8\{Ce_8(H_2O)_{20}\}(WO_2)_4(W_4O_{12})]^{48-}$. (b) $[Ce_{10}Te_8W_{88}O_{298}(OH)_{12}(H_2O)_{40}]^{18-}$. (c) $[\{Ln(H_2O)_5(TeW_{18}O_{64})\}_4]^{44-}$. (d) $[Ln_2(H_2O)_4(pica)_2W_2O_5][(Ln(H_2O)W_2(Hpica)_2O_4)(B\text{-}\beta\text{-}TeW_8O_{30}H_2)_2]^{24-}$. (e) $[Eu_4(H_2O)_4W_6(H_2glu)_4O_{12}(B\text{-}\alpha\text{-}TeW_9O_{33})_4]^{24-}$.

Fig. S2. The IR spectra of **1** and **nano-1**.

Fig. S3. Comparison of simulated and experimental PXRD patterns of **1** and **nano-1**.

Fig. S4. The TG curve of **1**.

Fig. S5. (a) The diffuse reflection spectrum of **nano-1.** (b) The optical band gap calculation of **nano-1**.

Fig. S6. (a) IR spectra of the **nano-1/NH_2-G** composites with different proportions of **nano-1** / **NH_2-G**. (b) PXRD patterns of the **nano-1/NH_2-G** composites with different proportions of **nano-1** / **NH_2-G**.

Fig. S7. Comparison of CV curves of the **nano-1/NH_2-G-GCE** with different proportions of **nano-1** / **NH_2-G** in 0.1 M PBS (pH = 6.5) containing 6 mM H_2O_2.

Fig. S8. (a) SEM image of **nano-1**. (b) SEM-EDS elemental mapping images of **nano-1** on tinfoil. (c) EDS of **nano-1**. (d-j) SEM-EDS W, O, P, C, Te, Ce and N elemental mapping images of **nano-1** on tinfoil.

Fig. S9. Raman spectra of various raw materials ($Na_2WO_4{\cdot}2H_2O$, K_2TeO_3, H_3PO_3), **1** and **nano-1**.

Fig. S10. CV curves of **nano-1/NH_2-G-GCE** in 0.1 M PBS containing 6 mM H_2O_2 at different pH values.

Fig. S11. CV curves of **nano-1/NH_2-G-GCE** in 0.1 M PBS (pH = 6.5) containing 6 mM H_2O_2 at different scan rates.

Fig. S12. Time-dependent stability of **nano-1/NH_2-G-GCE** in a period of seven days in 0.1 M PBS (pH = 6.5) containing 6 mM H_2O_2. The applied potential is –0.20 V.

Table S1. Crystallographic data and structure refinements for **1**.

Materials and physical measurements

All the chemicals and reagents are commercially purchased and used without further purification. K_2TeO_3, H_3PO_3, $Na_2WO_4{\cdot}2H_2O$, $Ce(NO_3)_3{\cdot}6H_2O$, 2-picolinic acid, dimethylamine hydrochloride, $K_3[Fe(CN)_6]$, $K_4[Fe(CN)_6]{\cdot}3H_2O$, KCl and H_2O_2 were purchased from Sparke Chemical Co. Ltd. (Zhengzhou, Henan Province). *β*-D-glucose (contains α-D-glucose) and glucose oxidase (50 KU, from Aspergillus Niger) are purchased from Aladdin. Phosphate buffer solutions (PBS) were prepared by mixing the stock solution of 0.1 M NaH_2PO_4 and 0.1 M Na_2HPO_4, and the pH was adjusted by using NaOH or HCl. C, H, and N elemental analyses were performed on a Vario EL Cube CHNS analyzer. Inductively coupled plasma atomic emission spectrometry (ICP–AES) was performed on a Perkin–Elmer Optima 2000 ICP–AES spectrometer. IR spectra were recorded on a Bruker VERTEX 70 IR spectrometer using KBr pellets in the range of 400–4000 cm^{-1}. PXRD patterns were collected on a Bruker D8 ADVANCE apparatus using Cu K*α* radiation (*λ* = 1.54056 Å) with a scan range (2θ) of 5–50° at 293 K. TG analysis was conducted under N_2 atmosphere on a Mettler-Toledo TGA/SDTA 851e thermal analyzer (temperature range: 25–1000°C; heating rate: 10°C·min^{-1}). SEM images and EDS patterns were obtained by FESEM, Zeiss Gemini 500. Raman spectra were obtained on a RM5 Raman microscope spectrometer with a 532 nm diode laser (EDINBUGH INSTRUMENTS). UV-vis spectra were obtained with a UH-4150 (Japan Hitashi) ultraviolet spectrophotometer.

X-ray crystallography

A good-quality single-crystal of **1** was picked carefully and its diffraction data were collected on a Bruker D8 Venture Photon II diffractometer equipped with CCD two-dimensional detector using monochromated Mo Kα radiation (λ = 0.71073 Å) at 296 K. Routine Lorentz and polarization corrections were applied and a multi-scan absorption correction was utilized with the SADABS program. Direct methods were used to solve the structure, refined on F^2 by full-matrix least-squares method using the SHELXTL–97 program.[1,2] All H atoms connected to N and C atoms were generated geometrically and refined isotropically as a riding model using the default SHELXTL parameters. No hydrogen atoms associated with water molecules are located from the difference Fourier map. All nonhydrogen atoms are refined anisotropically except for some sodium, carbon, oxygen atoms and water molecules. Based on the charge balance consideration, elemental analysis and TG analysis, one K^+ cation, one Na^+ cation, six protons and seventy-six lattice water molecules are directly added to each molecular formula of **1**. The crystallographic data and structure refinements for **1** is demonstrated in Table S1. Crystallographic data and structure refinements for **1** reported in this paper have been deposited in the Cambridge Crystallographic Data Centre with CCDC 2163291 for **1**. These data can be obtained free of charge from the Cambridge Crystallographic Data Centre via www.ccdc.cam.ac.uk/data_request/cif.

Preparation of nano-1

1.0 mg of **1** was dispersed in 5.0 mL ethanol solution under ultrasonication for 40 min. The **nano-1** solid was obtained by centrifugation, dried naturally and characterized by IR spectra and PXRD patterns.

Preparation of the nano-1/NH_2-G composites

NH_2-G (1.0, 0.5, 1.0, 1.5, 2.0 or 2.5 mg) was evenly dispersed in ethanol (1.0 mL) under ultrasonication for 45 min. **Nano-1** (1.0 mg) and ethanol (4.0 mL) were added to this solution and ultrasonication was continued for 40 min.

The mixture was heated in an oven at 85 °C for 2 days. The precipitate was obtained by centrifugation and dried overnight in a vacuum at 80°C. Finally, the **nano-1/NH_2-G** composites were obtained.

Preparation of nano-1/NH_2-G/GCE electrode

The **nano-1/NH_2-G** composite (4.0 mg), highly purified water (1.0 mL) and nafion (10.0 μL) were added to 2.0 mL centrifuge tube. After ultrasonication for 2 h, the resulting suspension (10.0 μL) was dropped onto the surface of the polished glassy carbon electrode (GCE). Then the **nano-1/NH_2-G-GCE** electrode was obtained and can be further used. The schematic preparation process of the **nano-1/NH_2-G-GCE** electrode is displayed in Scheme 1a–e.

Electrochemical measurements.

Electrochemical measurements were performed on a CHI66D electrochemical workstation (Chenhua Instruments, shanghai) with a conventional three electrode system, which consists of a modified GCE, a KCl-saturated Ag/AgCl reference electrode and a platinum counter electrode. When optimizing experimental conditions, the electrochemical performance of the modified GCE was tested in 0.1 mol/L PBS containing 6 mmol/L H_2O_2. The sweep speed (pH 6.5), potential (pH 6.5), different pH (pH 6.0, 6.5, 7.0, 7.5, 8.0), different electrodes (pH 6.5) and actual sample testing (pH 6.5) were measured in 0.1 mol/L PBS.

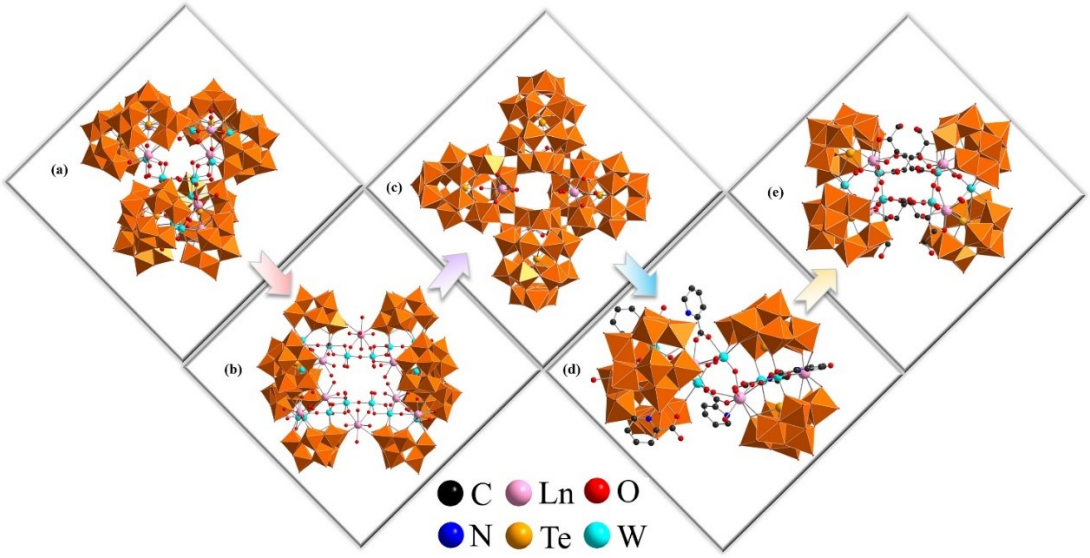

Fig. S1 Illustration of some typical HNLITTs. (a) $[\{(TeO_3)W_{10}O_{34}\}_8\{Ce_8(H_2O)_{20}\}(WO_2)_4(W_4O_{12})]^{48-}$. (b) $[Ce_{10}Te_8W_{88}O_{298}(OH)_{12}(H_2O)_{40}]^{18-}$. (c) $[\{Ln(H_2O)_5(TeW_{18}O_{64})\}_4]^{44-}$. (d) $[Ln_2(H_2O)_4(pica)_2W_2O_5][(Ln(H_2O)W_2(Hpica)_2O_4)(B\text{-}\beta\text{-}TeW_8O_{30}H_2)_2]^{24-}$. (e) $[Eu_4(H_2O)_4W_6(H_2glu)_4O_{12}(B\text{-}\alpha\text{-}TeW_9O_{33})_4]^{24-}$.

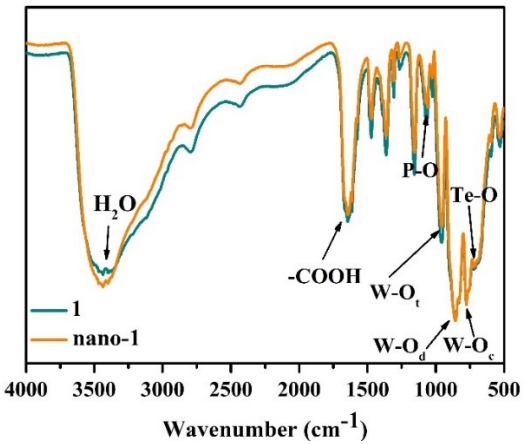

Fig. S2. The IR spectra of **1** and **nano-1**.

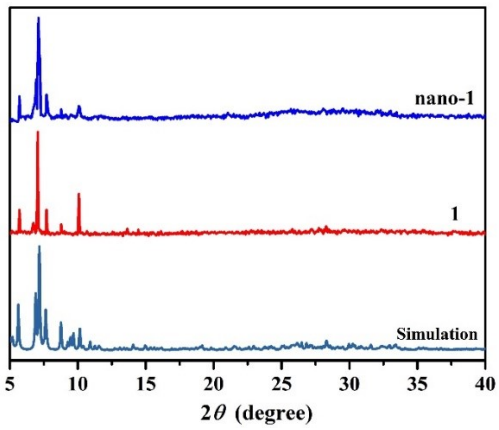

Fig. S3. Comparison of simulated and experimental PXRD patterns of **1** and **nano-1**.

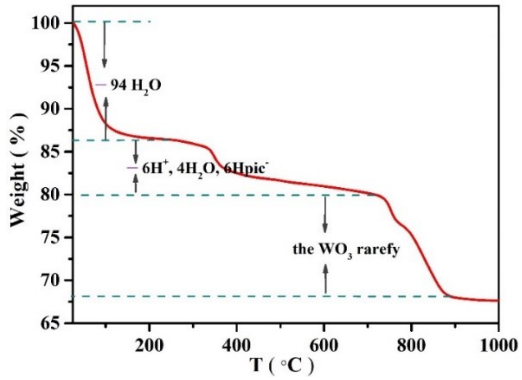

Fig. S4. The TG curve of **1**.

For the sake of investigating the thermal stability of **1**, the TG curve of **1** was collected under dry N_2 atmosphere ranging from 25 to 1000 °C (Fig. S4). It can be seen from the TG curve that the weight loss procedure of **1** can be divided into three steps: When temperature rises from 25°C to 250°C, the weight loss of **1** is 13.62% (calcd. 13.76%), which is attributed to the loss process of 94 lattice water molecules. In the process of temperature rising from 250°C to 700°C, the weight loss [6.73% (calcd. 7.06%)] of **1** is assigned to the loss of 4 coordination water molecules and 6 Hpica ligands and the dehydration of 6 protons. Subsequently, the skeleton of **1** begins to collapse as the temperature further increases and some of WO_3 begin to sublimate.

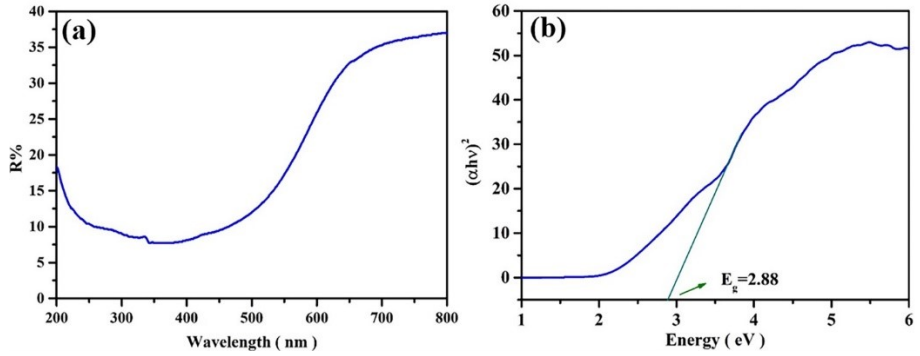

Fig. S5. (a) The diffuse reflection spectrum of **nano-1.** (b) The optical band gap calculation of **nano-1**.

The diffuse reflection spectrum (Fig. S5a) of **nano-1** was obtained. The band gap (E_g) was determined as the intersection point between the energy axis and the line extrapolated from the linear portion of the absorption edge in a plot of Kubelka-Munk function against energy *E.* Kubelka-Munk function, $a/S = (1–R)^2/2R$, was converted from the recorded diffuse reflectance data, where a is the absorption coefficient, S is the scattering coefficient, R is the reflectance of an infinitely thick layer at a given wavelength. The plot of Kunelka-Munk function versus energy E (eV) for **nano-1** is shown in (Fig. S5b), where the steep absorption edge is displayed, from which E_g can be assessed at E_g = 2.88 eV for **nano-1**.

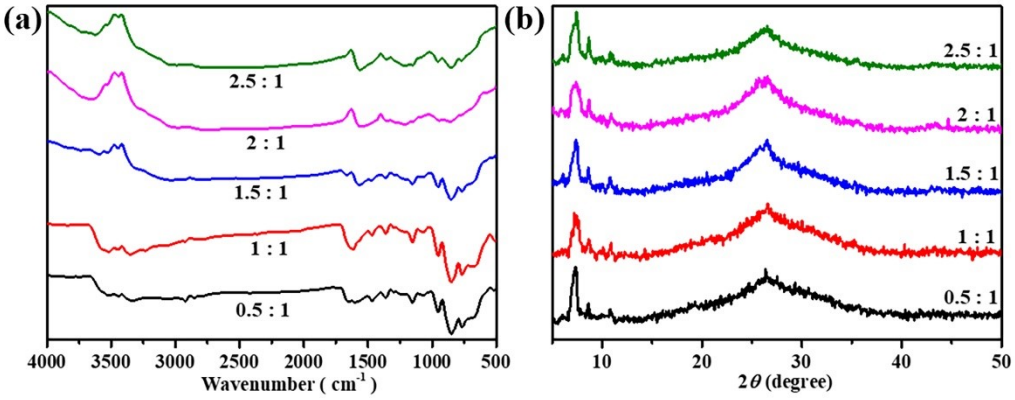

Fig. S6. (a) IR spectra of the **nano-1/NH_2-G** composites with different proportions of **nano-1** / **NH_2-G**. (b) PXRD patterns of the **nano-1/NH_2-G** composites with different proportions of **nano-1** / **NH_2-G**.

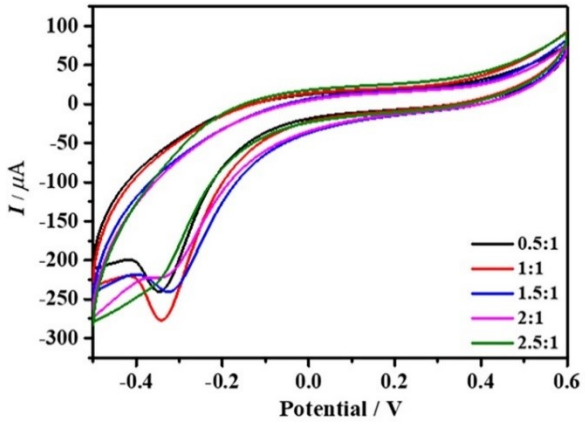

Fig. S7. Comparison of CV curves of the **nano-1/NH_2-G-GCEs** with different proportions of **nano-1** / **NH_2-G** in 0.1 M PBS (pH = 6.5) containing 6 mM H_2O_2.

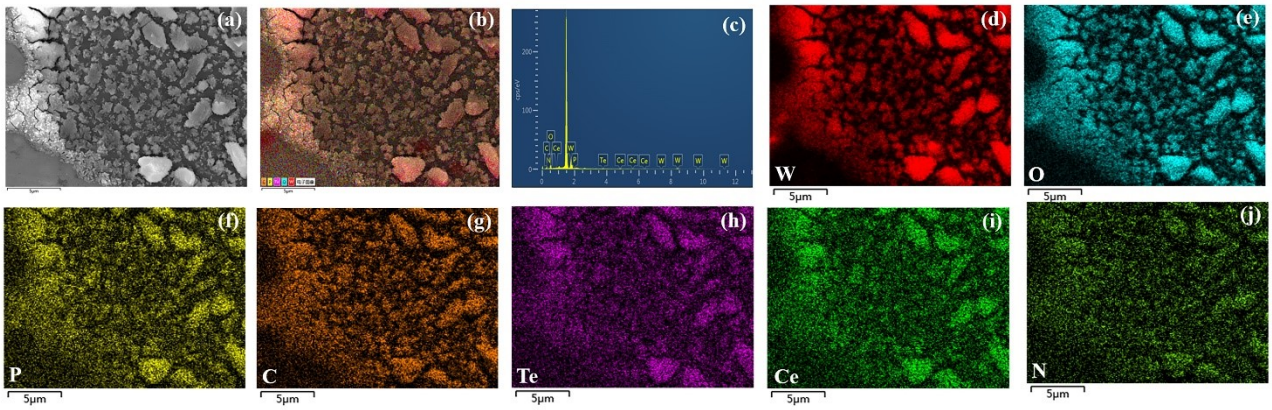

Fig. S8. (a) SEM image of **nano-1**. (b) SEM-EDS elemental mapping images of **nano-1** on tinfoil. (c) EDS of **nano-1**. (d-j) SEM-EDS W, O, P, C, Te, Ce and N elemental mapping images of **nano-1** on tinfoil.

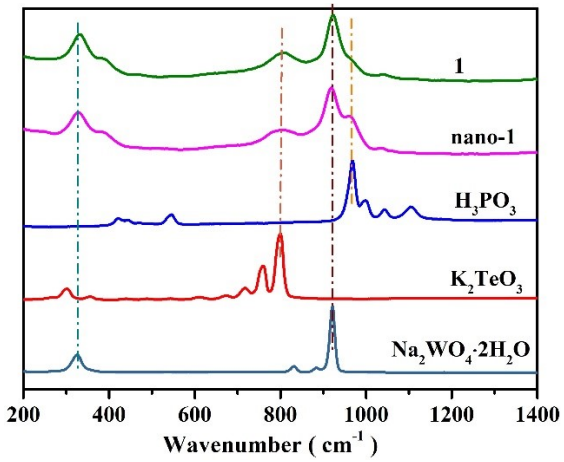

Fig. S9. Raman spectra of various raw materials ($Na_2WO_4{\cdot}2H_2O$, K_2TeO_3, H_3PO_3), **1** and **nano-1**.

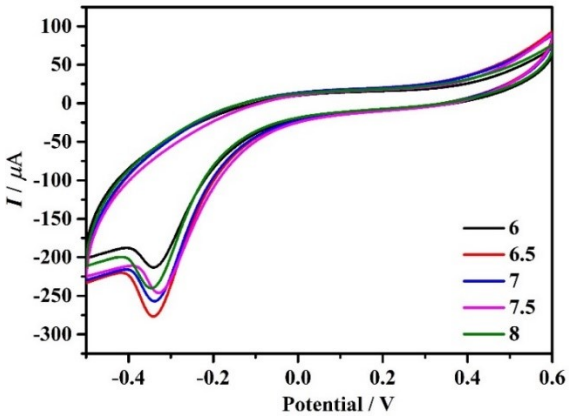

Fig. S10. CV curves of **nano-1/NH_2-G-GCE** in 0.1 M PBS containing 6 mM H_2O_2 at different pH values.

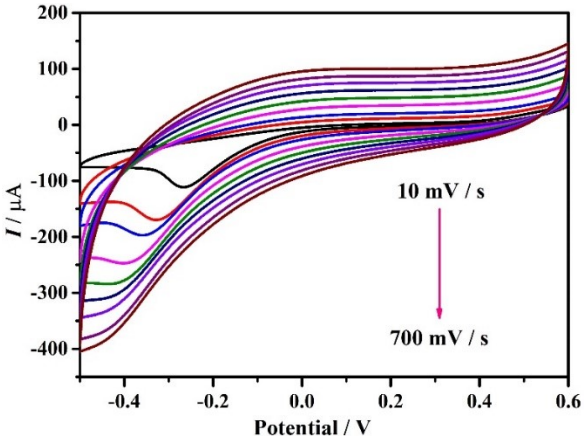

Fig. S11. CV curves of **nano-1/NH_2-G-GCE** in 0.1 M PBS (pH = 6.5) containing 6 mM H_2O_2 at different scan rates.

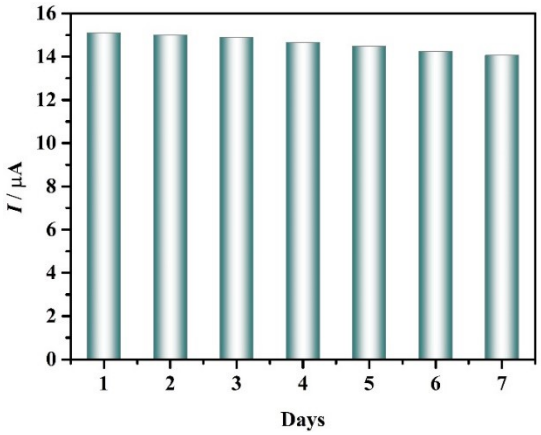

Fig. S12. Time-dependent stability of **nano-1/NH_2-G-GCE** in a period of seven days in 0.1 M PBS (pH = 6.5) containing 6 mM H_2O_2. The applied potential is –0.20 V.

Table S1. Crystallographic data and structure refinements for **1.**

	1
Empirical formula	$C_{36}H_{234}Ce_5K_3N_6Na_4O_{238}P_2Te_4W_{34}$
Formula weight	12293.39
T, (K)	150(2)
Crystal system	monoclinic
Space group	*C*2/*c*
a, (Å)	20.6357(8)
b, (Å)	46.272(2)
c, (Å)	31.6865(15)
α, (deg)	90
β, (deg)	97.4420(10)
γ, (deg)	90
V ($Å^{-3}$)	30001(2)
Z	4
Dc, ($g·cm^{-3}$)	2.722

μ (mm^{-1})	14.258
Limiting indices	$-24 \le h \le 24$
	$-47 \le k \le 55$
	$-36 \le l \le 37$
GOF on F^2	1.032
R_1, wR_2 ($I > 2\sigma(I)$)[a]	$R_1 = 0.0768$, $wR_2 = 0.2249$
R_1, wR_2 (all data)	$R_1 = 0.1500$, $wR_2 = 0.2679$

References

1 G. M. Sheldrick, SHELXL-97, Program for Crystal Structure Refinement, University of Göttingen: Göttingen, Germany, 1997.

2 G. M. Sheldrick, SHELXS-97, Program for Crystal Structure Solution, University of Göttingen: Göttingen, Germany, 1997.